Hindawi
Wireless Communications and Mobile Computing
Volume 2018, Article ID 1729121, 7 pages
https://doi.org/10.1155/2018/1729121

Research Article

Analysis of Nonstationary Characteristics for High-Speed Railway Scenarios

Tao Zhou,[1,2] **Cheng Tao**,[1] **and Kai Liu**[1]

[1]*Institute of Broadband Wireless Mobile Communications, Beijing Jiaotong University, Beijing 100044, China*
[2]*National Mobile Communications Research Laboratory, Southeast University, Nanjing 210096, China*

Correspondence should be addressed to Tao Zhou; taozhou.china@gmail.com

Received 21 March 2018; Accepted 29 May 2018; Published 21 June 2018

Academic Editor: Tommi Jamsa

This paper presents the analysis of nonstationary characteristics for high-speed railway (HSR) scenarios, according to passive long-term evolution- (LTE-) based channel measurements. The measurement data collected in three typical scenarios, rural, station, and suburban, are processed to obtain the channel impulse responses (CIRs). Based on the CIRs, the nonstationarity of the HSR channel is studied focusing on the stationarity interval, and a four-state Markov chain model is generated to describe the birth-death process of multipath components. The presented results will be useful in dynamic channel modeling for future HSR mobile communication systems.

1. Introduction

With the rapid development of high-speed railways (HSRs), there appears a growth in demand for new railway communication services, for example, real-time monitoring, train multimedia dispatching, railway emergency communications, railway Internet of Things (IoT), and broadband wireless access for train passengers [1]. To satisfy such ever-increasing requirements, broadband wireless communication systems for HSR have recently attracted much attention in the world. Since 2014, International Union of Railways (UIC) has considered replacing the current global system for mobile communications for railway (GSM-R) with the long-term evolution for railway (LTE-R) [2]. In China, fourth-generation (4G) networks have been deployed along most of HSRs, for a total of 15,000 km by 2014, and as HSRs continue to grow, the dedicated 4G networks that grow with them will exceed 30,000 km in 2020. For future fifth-generation (5G) mobile communication system, it is reported that one of its aims is to provide high-data-rate access under high mobility scenarios [3].

Since the radio channel determines the performance of broadband wireless mobile communication systems, detailed knowledge and accurate characterization of its parameters in diverse scenarios are vital. The propagation characteristics are in disparity under various HSR environments. In this case, the characterization of HSR channels should consider the influence of scenarios.

So far, a wide variety of the studies have concentrated on the long-term fading behavior, involving path loss and shadowing, in multiple HSR scenarios [4–8]. There are a few research works on the short-term fading behavior, based on wideband channel measurements conducted on HSR. By contrast, the nonstationary behavior, which has been widely studied for vehicle-to-vehicle (V2V) channels [9, 10], is rarely investigated in HSR environments. To fill this research gap, we present the analysis of the nonstationary characteristics for multiple HSR scenarios. Passive channel measurements are conducted for three typical scenarios, rural, station, and suburban, in an HSR LTE network. Considering the interval of stationarity and the dynamic evolution of multipath components (MPCs), the nonstationary behavior is analyzed and compared in different scenarios.

The remainder of this paper is outlined as follows. Section 2 reviews the related work focusing on short-term fading and nonstationary behaviors. In Section 3, our passive channel measurements based on LTE are introduced. Then, the nonstationary characteristics are analyzed in Section 4, respectively. Finally, conclusions are drawn in Section 5.

Table 1: Summary of investigation on short-term fading and nonstationary behaviors in HSR environments.

Scenario	Short-term fading behavior				Nonstationary behavior	
	Fading severity	Time dispersion	Frequency dispersion	Space dispersion	Stationarity interval	Birth-death process
Viaduct	[11, 12, 16]	[11]	[11, 12]	[15]	[25]	[26]
Cutting	[13, 14, 17]	[13, 14]	[13, 14]	[15]	-	-
Rural	[18]	[18, 19]	[19]	[18, 19]	-	-
Hilly terrain	[20]	[21]	[21]	-	-	-
Tunnel	[22]	[22]	[22]	-	-	-
Station	[23, 24]	[24]	-		[24]	-
Suburban/urban	-	-	-	-	-	-

2. Related Work

Unique HSR scenarios, such as viaduct, cutting, tunnel, station, hilly terrain, rural, and suburban, have a significant impact on propagation characteristics. In our previous work, fading severity and time-frequency-space dispersion of HSR channels in the viaduct and cutting scenarios were deeply characterized based on measurements using Propsound [11–15]. In [15], spatial characteristics, involving angle of arrival (AOA), root-mean-square (RMS) angle spread (AS), and spatial correlation (SC), were analyzed according to a so-called moving virtual antenna array (VAA) scheme. Authors in [16, 17] proposed a statistic model for Ricean K-factor, which investigated the impact of the viaduct height and the cutting width. The WINNER II model [18] and COST 2100 TD [19] provided some measurement results of short-term fading behavior for rural scenarios. There were also a few results of K-factor, RMS delay spread (DS), and Doppler power spectral density (DPSD) measured in the hilly terrain and tunnel scenarios [20–22]. Authors in [23, 24] presented detailed analysis of fading severity and time dispersion in open-type and semiclosed station scenarios. For the nonstationary behavior, stationarity interval (SI) in the viaduct scenario was investigated based on GSM-R measurements, which showed that conventional channel models offered SI much larger than the actual measured ones [25]. We also tried to adopt a RUN test method to obtain the SI for the open-type station scenario in [24]. Additionally, a four-state Markov chain was used to model the birth-death (B-D) process of MPCs in the viaduct scenario [26].

Table 1 summarizes the existing measurement campaigns about short-term fading and nonstationary behaviors in different HSR environments. It can be found that there are a few results of time-frequency-space characteristics in some HSR scenarios. However, the characterization of the nonstationary behavior is largely neglected in most scenarios. Therefore, this paper aims to investigate the nonstationary behavior in the rural, station, and suburban scenarios.

3. Channel Measurements

3.1. Measurement Scenarios. An LTE network deployed on Beijing to Tianjin (BT) HSR in China was chosen in our measurements [27]. It is a hybrid network composed of a dedicated network and a common network. The architecture of the dedicated network is completely different from the common network, which adopts building baseband unit (BBU) plus remote radio unit (RRU) to achieve the special narrow-strip-shaped coverage instead of the cellular coverage. In this architecture, one physical site (PS) deploys two RRUs, which transmit signals by directional antennas in opposite directions along the railway track. The RRUs are connected together via optical fiber and then to a BBU that is in charge of radio frequency (RF) signal processing.

Table 2: Measurement parameters in the BT HSR LTE network.

Scenario	Rural	Station	Suburban
eNB side			
Frequency	1.89 GHz		2.605 GHz
Bandwidth	18 MHz		18 MHz
CRS power	12.2 dBm		12.2 dBm
Antenna type	Directional		Directional
Antenna gain	17.4 dBi		18.6 dBi
Horizontal beamwidth	67 deg		60 deg
Vertical beamwidth	6.6 deg		4.9 deg
Electric tilted angle	3 deg		3 deg
Sounder side			
Antenna type	Omnidirectional		Omnidirectional
Antenna gain	8.5 dBi		8.5 dBi
Speed of HST	285 km/h		185 km/h
Network side			
Distance between PSs	1.2 km		
Height of PS	30 m		
Height of rail track	10 m		
Distance between PS and rail track	30 m		

The LTE sounder is placed on a high-speed train (HST) to collect the channel data, which experiences multiple scenarios along the BT railway line, such as rural, station, and suburban. In our measurement, the rural and station scenarios are within the coverage of dedicated network, while the suburban scenario is covered by the common network. The detailed measurement parameters for different scenarios in the network are listed in Table 2. The carrier frequency is 1.89 GHz for the rural and station scenarios and 2.605 GHz for the suburban scenario. When the HST moves into

(a) (b) (c)

Figure 1: Measurement scenarios. (a) Rural. (b) Station. (c) Suburban.

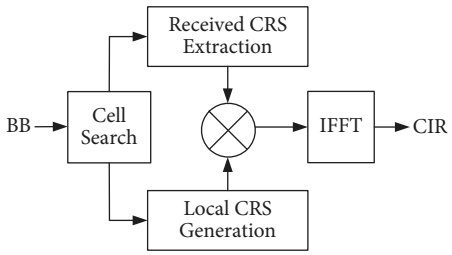

Figure 2: The procedure of data processing.

the suburban area, the speed is decreased from 285 km/h to 185 km/h. The specification of the directional eNB antenna such as gain and beamwidth has slight difference in different frequencies. At Rx side, the LTE sounder is connected to a train-mounted omnidirectional antenna. The average spacing between neighboring PSs is around 1.2 km. The height and distance difference between the PS and the rail track are about 20 m and 30 m, respectively.

The measured scenarios are shown in Figure 1. As for the rural scenario, the transmit antenna is much higher than the surroundings, which are light forests and a few buildings with an average height of less than 10 m. The link between the transmitter (Tx) and Rx generally has a strong line-of-sight (LoS) component. However, after a certain distance, the impact of the sparse scatterers will be noticed at the Rx represented by non-LoS (NLoS) components. With regard to the station scenario, in the measurement, the HST runs through the station without stopping. The measured station can be regarded as an open-type station with two awnings that only cover the platform supporting a clear free space over the rail. However, the awnings can still produce lots of NLoS components to complicate the fading behavior. The length of the station is 440 m, the width of the awning is 14 m, and the width of the gap between the two awnings is 9 m. Suburban is a transition zone between the rural and urban. The NLoS components in the suburban environment will be much richer than those in the rural environment. The density of the buildings in the suburban scenario is similar to that in the urban scenario, but the height of the buildings is lower. Since the measured suburban is close to the urban area, some remote high buildings could affect the results.

3.2. Data Processing. Baseband data (BB) collected by the LTE sounder in the multilink regions are used for offline processing. The procedure of data processing is shown in Figure 2. Firstly, cell search is implemented to determine the cell identity and obtain synchronized frames for extracting received CRSs and generating local CRSs. Then, frequency-domain correlation is used to estimate channel frequency responses which can be subsequently transformed to the raw CIRs by inverse fast Fourier transform (IFFT) operation [28].

4. Results and Analysis

4.1. Stationarity Interval. High mobility leads to the violation of wide sense stationary (WSS) condition for wireless channels under HSR scenarios. The stationarity interval (SI) is defined as the maximum time or distance duration, over which the channel satisfies the WSS condition. It is summarized by [29] that there are several metrics that can be used for measuring the SI, involving local region of stationarity (LRS), correlation matrix distance (CMD), and spectral divergence (SD). Besides, some statistical tests for the WSS of a random process can also be applied to the determination of SI, such as RUN test and reverse arrangement test. The LRS method has been used to estimate the time interval of HSR channels in [25]. The RUN test was applied to the RMS DS data to identify the stationary distance in the station scenario [24]. In this paper, we choose the classical LRS approach to characterize the SI in the measured scenarios.

The aim of the LRS method is to find the maximum interval within which the correlation coefficient between two consecutive PDPs exceeds a predefined threshold c_{th}. The correlation coefficient between PDPs is defined as

$$c\left(x_k, \Delta x\right) = \frac{\overline{P\left(x_k\right)}\,\overline{P\left(x_k + \Delta x\right)}}{\max\left\{\overline{P\left(x_k\right)}^2, \overline{P\left(x_k + \Delta x\right)}^2\right\}}, \tag{1}$$

where

$$\overline{P\left(x_k\right)} = \frac{1}{N}\sum_{m=k}^{k+N-1}\left|h\left(x_m\right)\right|^2, \tag{2}$$

where N is the window size and $h(x_m)$ are the samples of channel impulse response.

Then, the SI can be estimated as

$$I_k = \left(k_{\max} - k_{\min}\right)\Delta x \tag{3}$$

where

$$k_{\max} = \underset{k+1\le m\le L-N}{\arg\max}\; c\left(x_k, m\Delta x\right) < c_{th} \tag{4}$$

$$k_{\min} = \underset{1\le m\le k-1}{\arg\min}\, c\left(x_k, m\Delta x\right) < c_{th} \tag{5}$$

Table 3: Analysis results of the SI in different scenarios.

Scenario	Method	Statistics	SI (m)		
			c_{th} = 0.7	c_{th} = 0.8	c_{th} = 0.9
Rural	LRS	Mean value	14.3	6.46	2.84
		60% of CCDF	8.22	4.29	1.65
		80% of CCDF	4.74	2.64	0.99
Station	LRS	Mean value	7.27	3.84	1.87
		60% of CCDF	5.02	2.55	1.17
		80% of CCDF	3.07	1.25	0.37
Suburban	LRS	Mean value	7.62	3.74	1.37
		60% of CCDF	5.43	2.33	0.86
		80% of CCDF	3.54	1.25	0.35
Viaduct [26]	LRS	60% of CCDF	-	1.8	-
		80% of CCDF	-	0.81	-
Standard models [26]	LRS	60% of CCDF	-	3.4	-
Station [25]	RUN test	80% of CCDF		4	

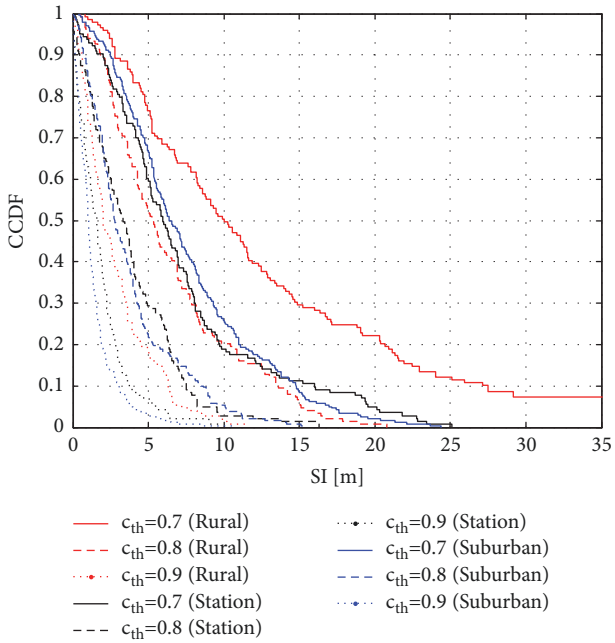

Figure 3: CCDFs of SI in rural, station, and suburban scenarios.

where L is the length of used data. Here, we consider three typical correlation threshold values: c_{th} = 0.7, c_{th} = 0.8, and c_{th} = 0.9.

Figure 3 compares the derived SI results for different c_{th} and scenarios in terms of complementary CDF (CCDF). With the increase of c_{th}, the SI is gradually decreasing. For c_{th} = 0.9, only slight difference can be observed in different environments, while there is an obvious deviation for c_{th} = 0.7 and c_{th} = 0.8. Focusing on the cases of c_{th} = 0.7 and c_{th} = 0.8, we find that the SI values in the rural scenario are larger than those in the station or suburban scenarios. This is understandable from the completely different scattering environment. Since LoS is dominant in the rural scenario, the MPCs have smaller dynamic changes over time, and thus the stationary distance is longer. When it comes to the station and suburban scenarios, due to the rich reflection and scattering components from the awnings or buildings, the nonstationarity is more serious, and thus the SI decreases. This nonstationarity could be originated from a special physical phenomena, for example, "appearance and disappearance" or "birth and death" of MPCs [26], which will be further investigated in the following subsection.

The detailed statistical SI results including mean value and 60% and 80% of CCDF for different scenarios are listed in Table 3. For c_{th} = 0.8, the mean value of SI is 6.46 m in the rural scenario, while those are 3.84 m and 3.74 m in the station and suburban scenarios. In 60% and 80% of cases, the channel could be stationary over a distance of 2.33-4.29 m and 1.25-2.64 m for the measured scenarios, respectively. These values are higher than the results of 1.8 m for 60% and 0.81 m for 80% reported in [25]. From [25], the calculated stationary interval for standard channel models is equal to 3.4 m for 60%, which is shorter than the one of 4.29 m for the rural scenario but is longer than the ones of 2.55 m and 2.33 m for the station and suburban scenarios. It is also observed that the value of SI in 80% of the cases in the measured station scenario is smaller than that of around 4 m in the station scenario reported in [24]. This variance could be due to the use of different calculation methods.

4.2. Birth-Death Process. The nonstationarity of the channel is basically due to the dynamic evolution of MPCs when the Rx is in motion, for example, appearance to disappearance or B-D. To describe this B-D process, a four-state Markov chain model (MCM) is used, where each state is defined as follows [30]:

(i) S_0: no "births" or "deaths"

(ii) S_1: "births" only

(iii) S_2: "deaths" only

(iv) S_3: both "births" and "deaths"

Table 4: Analysis results of the B-D process in different scenarios.

Scenario	State transition probability matrix	Steady-state probability
Rural	$\begin{bmatrix} 0.3361 & 0.4025 & 0.1203 & 0.1411 \\ 0.0497 & 0.0315 & 0.5348 & 0.3841 \\ 0.1658 & 0.7148 & 0.0282 & 0.0912 \\ 0.0332 & 0.0600 & 0.2505 & 0.6563 \end{bmatrix}$	$\begin{bmatrix} 0.1017 & 0.2533 & 0.2530 & 0.3920 \end{bmatrix}$
Station	$\begin{bmatrix} 0.2791 & 0.2093 & 0.1628 & 0.3488 \\ 0.0224 & 0.0096 & 0.4936 & 0.4744 \\ 0.0354 & 0.7235 & 0.0129 & 0.2283 \\ 0.0081 & 0.0471 & 0.0905 & 0.8544 \end{bmatrix}$	$\begin{bmatrix} 0.0189 & 0.1374 & 0.1366 & 0.7071 \end{bmatrix}$
Suburban	$\begin{bmatrix} 0.1870 & 0.2439 & 0.1463 & 0.4228 \\ 0.0557 & 0.0557 & 0.2256 & 0.6630 \\ 0.0780 & 0.4150 & 0.0613 & 0.4457 \\ 0.0151 & 0.0464 & 0.0690 & 0.8695 \end{bmatrix}$	$\begin{bmatrix} 0.0287 & 0.0837 & 0.0837 & 0.8039 \end{bmatrix}$
Viaduct [17]	$\begin{bmatrix} 0.2917 & 0.5208 & 0.1667 & 0.0208 \\ 0.0200 & 0.1000 & 0.5200 & 0.3600 \\ 0.2577 & 0.4330 & 0.0928 & 0.2165 \\ 0.0673 & 0.2115 & 0.2788 & 0.4423 \end{bmatrix}$	$\begin{bmatrix} 0.1371 & 0.2800 & 0.2857 & 0.2971 \end{bmatrix}$

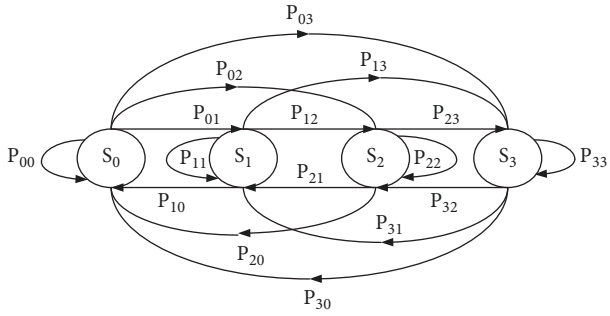

Figure 4: State transition diagram of the four-state MCM.

Note that the state in the MCM only considers the variation of MPCs from the current moment to the next moment. With the motion of the Rx, the states can be transformed to each other. Figure 4 illustrates the state transition diagram of the four-state MCM [30]. The probabilistic switching process between states in the MCM is controlled by the state transition probability matrix $\mathbf{P}$ given by

$$\mathbf{P} = \{p_{ij}\} = \begin{bmatrix} p_{00} & p_{01} & p_{02} & p_{03} \\ p_{10} & p_{11} & p_{12} & p_{13} \\ p_{20} & p_{21} & p_{22} & p_{23} \\ p_{30} & p_{31} & p_{32} & p_{33} \end{bmatrix} \tag{6}$$

where i and j represent the state index, while p_{ij} is the transition probability from state S_i to state S_j. Note that p_{ij} must satisfy the following requirement:

$$0 \le p_{ij} \le 1, \quad i, j = 0, 1, \ldots, N-1 \tag{7}$$

$$\sum_{j=0}^{N-1} p_{ij} = 1, \quad i = 0, 1, \ldots, N-1 \tag{8}$$

where N is the number of states; that is, $N = 4$ in our case.

The steady-state probability can be expressed as

$$\mathbf{P}_S = \begin{bmatrix} P_{S_0} & P_{S_1} & P_{S_2} & P_{S_3} \end{bmatrix} \tag{9}$$

which satisfies $P_{S_0} + P_{S_1} + P_{S_2} + P_{S_3} = 1$. Each element in $\mathbf{P}_S$ indicates the overall state occupancy probability.

The obtained results of the state transition probability matrix in different scenarios are listed in Table 4. Here, the state transition matrix is derived from each CIR. Since the sample rate of CIR is 2000 Hz and the velocity of train is 79 m/s, the reference value for state transition matrix is 0.04 m. It is observed that in the suburban scenario the next state is more likely to transit into the state S_3 no matter what the current state is S_0, S_1, or S_2. This means some new MPCs are born and older MPCs die most of the time because of the rich reflection and scattering components in the suburban scenario. For other scenarios, in the case of S_0, the next state could be any one of the four states; in the case of S_1, S_2 or S_3 have the maximum probability to be the next state; in the case of S_2, the next state is more likely to transit into S_1; in the case of S_3, the next state is still likely to be S_3. The results show the nonsymmetric transition matrix, which means that the transition probability from state A to state B has no relationship with that from state B to state A.

According to the state transition probability matrix, the steady-state probability can be derived, as listed in Table 4. It is found that S_3 is the most likely state in the station and suburban scenarios. For the rural scenario, either S_1, S_2,

or S_3 could be the steady state. It is worth noting that S_1 and S_2 have approximately similar steady-state probability in any scenario. This confirms that the appearance and disappearance of MPCs are equivalent. The above results in the rural scenario are similar to those in the open viaduct scenario reported in [26]. The obtained results can be applied for ON/OFF tapped delay line models that use the Markov chain to model the ON/OFF process of MPCs [31].

5. Conclusion

This paper analyzes the nonstationary characteristics in typical HSR scenarios, rural, station, and suburban, depending on the passive LTE-based channel measurements. With regard to the nonstationary characteristics, it is found that the SI is longest in the rural scenario. Additionally, a four-state MCM is established to characterize the B-D process of MPCs, and the corresponding state transition probability matrix and steady-state probability are provided. These results show the realistic channel characteristics in the HSR communication network, which will provide helpful information for nonstationary channel modeling of HSR communication systems.

Data Availability

The data used to support the findings of this study are available from the corresponding author upon request.

Conflicts of Interest

The authors declare that they have no conflicts of interest.

Acknowledgments

This work was supported by the Fundamental Research Funds for the Central Universities (Grant 2018JBZ102), the National Natural Science Foundation of China (Grant 61701017), the Beijing Municipal Natural Science Foundation (Grant 4174102), and the Open Research Fund through the National Mobile Communications Research Laboratory, Southeast University (Grant 2018D11).

References

[1] R. He, B. Ai, G. Wang et al., "High-Speed railway communications: from GSM-R to LTE-R," *IEEE Vehicular Technology Magazine*, vol. 11, no. 3, pp. 49–58, 2016.

[2] B. Ai, X. Cheng, T. Kurner et al., "Challenges toward wireless communications for high-speed railway," *IEEE Transactions on Intelligent Transportation Systems*, vol. 15, no. 5, pp. 2143–2158, 2014.

[3] *White Paper for 5G High Mobility*, [Online], Available, http://www.future-forum.org.

[4] H. Wei, Z. Zhong, K. Guan, and B. Ai, "Path loss models in viaduct and plain scenarios of the High-speed Railway," in *Proceedings of the 5th International ICST Conference on Communications and Networking in China*, Beijing, China, August 2010.

[5] R. He, Z. Zhong, B. Ai, and J. Ding, "An empirical path loss model and fading analysis for high-speed railway viaduct scenarios," *IEEE Antennas and Wireless Propagation Letters*, vol. 10, pp. 808–812, 2011.

[6] K. Guan, Z. Zhong, B. Ai, and T. Kurner, "Empirical models for extra propagation loss of train stations on high-speed railway," *IEEE Transactions on Antennas and Propagation*, vol. 62, no. 3, pp. 1395–1408, 2014.

[7] R. He, Z. Zhong, B. Ai, and C. Oestges, "Shadow fading correlation in high-speed railway environments," *IEEE Transactions on Vehicular Technology*, vol. 64, no. 7, pp. 2762–2772, 2015.

[8] L. Liu, C. Tao, D. W. Matolak, T. Zhou, and H. Chen, "Investigation of Shadowing Effects in Typical Propagation Scenarios for High-Speed Railway at 2350 MHz," *International Journal of Antennas and Propagation*, vol. 2016, pp. 1–8, 2016.

[9] O. Renaudin, V.-M. Kolmonen, P. Vainikainen, and C. Oestges, "Non-stationary narrowband MIMO inter-vehicle channel characterization in the 5-GHz band," *IEEE Transactions on Vehicular Technology*, vol. 59, no. 4, pp. 2007–2015, 2010.

[10] D. W. Matolak, "Modeling the vehicle-to-vehicle propagation channel: A review," *Radio Science*, vol. 49, no. 9, pp. 721–736, 2014.

[11] L. Liu, C. Tao, J. Qiu et al., "Position-based modeling for wireless channel on high-speed railway under a viaduct at 2.35 GHz," *IEEE Journal on Selected Areas in Communications*, vol. 30, no. 4, pp. 834–845, 2012.

[12] T. Zhou, C. Tao, L. Liu, and Z. Tan, "A semiempirical MIMO channel model in obstructed viaduct scenarios on high-speed railway," *International Journal of Antennas and Propagation*, vol. 2014, Article ID 287159, 10 pages, 2014.

[13] T. Zhou, C. Tao, S. Salous, Z. Tan, L. Liu, and L. Tian, "Graph-based stochastic model for high-speed railway cutting scenarios," *IET Microwaves, Antennas & Propagation*, vol. 9, no. 15, pp. 1691–1697, 2015.

[14] R. Sun, C. Tao, L. Liu, and Z. Tan, "Channel Measurement and Characterization for HSR U-Shape Groove Scenarios at 2.35 GHz," in *Proceedings of the 2013 IEEE 78th Vehicular Technology Conference (VTC Fall)*, pp. 1–5, Las Vegas, NV, USA, September 2013.

[15] T. Zhou, C. Tao, S. Salous, and L. Liu, "Spatial Characterization for High-Speed Railway Channels Based on Moving Virtual Array Measurement Scheme," *IEEE Antennas and Wireless Propagation Letters*, vol. 16, pp. 1423–1426, 2017.

[16] R. He, Z. Zhong, B. Ai, G. Wang, J. Ding, and A. F. Molisch, "Measurements and analysis of propagation channels in high-speed railway viaducts," *IEEE Transactions on Wireless Communications*, vol. 12, no. 2, pp. 794–805, 2013.

[17] R. He, Z. Zhong, B. Ai, J. Ding, Y. Yang, and A. F. Molisch, "Short-term fading behavior in high-speed railway cutting scenario: Measurements, analysis, and statistical models," *IEEE Transactions on Antennas and Propagation*, vol. 61, no. 4, pp. 2209–2222, 2013.

[18] P. Kyösti et al., *WINNER II channel models part II radio channel measurement and analysis results*, vol. ST-4-027756, 2007, WINNER II D1.1.2, v1.0.

[19] R. Parviainen, P. Ky, Y. Hsieh, P. Ting, and J. Chiou, "Results of high speed train channel measurements , in," in *Proc. COST 2100 TD*, France, Lille, 2008.

[20] F. Luan, Y. Zhang, L. Xiao, C. Zhou, and S. Zhou, "Fading characteristics of wireless channel on high-speed railway in hilly terrain scenario," *International Journal of Antennas and Propagation*, vol. 2013, Article ID 378407, 9 pages, 2013.

[21] Y. Zhang, Z. He, W. Zhang, L. Xiao, and S. Zhou, "Measurement-based delay and doppler characterizations for high-speed railway hilly scenario," *International Journal of Antennas and Propagation*, vol. 2014, Article ID 875345, 8 pages, 2014.

[22] P. Aikio, R. Gruber, and P. Vainikainen, "Wideband radio channel measurements for train tunnels," in *Proceedings of the VTC '98. 48th IEEE Vehicular Technology Conference. Pathway to a Global Wireless Revolution*, pp. 460–464, Ottawa, Ont., Canada.

[23] K. Guan, Z. Zhong, B. Ai, and T. Kürner, "Propagation measurements and modeling of crossing bridges on high-speed railway at 930 MHz," *IEEE Transactions on Vehicular Technology*, vol. 63, no. 8, pp. 3349–3516, 2014.

[24] T. Zhou, C. Tao, S. Salous, L. Liu, and Z. Tan, "Channel characterization in high-speed railway station environments at 1.89 GHz," *Radio Science*, vol. 50, no. 11, pp. 1176–1186, 2015.

[25] B. Chen, Z. Zhong, and B. Ai, "Stationarity intervals of time-variant channel in high speed railway scenario," *China Communications*, vol. 9, no. 8, pp. 64–70, 2012.

[26] L. Liu, C. Tao, J. Qiu, T. Zhou, R. Sun, and H. Chen, "The dynamic evolution of multipath components in High-Speed Railway in viaduct scenarios: From the birth-death process point of view," in *Proceedings of the 2012 IEEE 23rd International Symposium on Personal, Indoor and Mobile Radio Communications - (PIMRC 2012)*, pp. 1774–1778, Sydney, Australia, September 2012.

[27] T. Zhou, C. Tao, S. Salous, L. Liu, and Z. Tan, "Channel sounding for high-speed railway communication systems," *IEEE Communications Magazine*, vol. 53, no. 10, pp. 70–77, 2015.

[28] T. Zhou, C. Tao, S. Salous, L. Liu, and Z. Tan, "Implementation of an LTE-based channel measurement method for high-speed railway scenarios," *IEEE Transactions on Instrumentation and Measurement*, vol. 65, no. 1, pp. 25–36, 2016.

[29] R. He, O. Renaudin, V.-M. Kolmonen et al., "Characterization of quasi-stationarity regions for vehicle-to-vehicle radio channels," *IEEE Transactions on Antennas and Propagation*, vol. 63, no. 5, pp. 2237–2251, 2015.

[30] C.-C. Chong, C.-M. Tan, D. I. Laurenson, S. McLaughlin, M. A. Beach, and A. R. Nix, "A novel wideband dynamic directional indoor channel model based on a Markov process," *IEEE Transactions on Wireless Communications*, vol. 4, no. 4, pp. 1539–1552, 2005.

[31] I. Sen and D. Matolak, "Vehicle channel models for the 5-ghz band," *IEEE T. Intell. Transp*, vol. 9, no. 2, pp. 235–245, June 2008.